J Theor Appl Phys (2017) 11:37–43
DOI 10.1007/s40094-016-0234-8

RESEARCH

Experimental and theoretical study on the corrosion resistance of Zr–Co–Al–Nb metallic glasses

W. K. Le[1] · Z. Z. Yuan[1] · X. Y. Zhang[1]

Received: 20 April 2016 / Accepted: 22 October 2016 / Published online: 3 November 2016

Abstract The corrosion resistance of $(Zr_{56}Al_{16}Co_{28})_{100-X}Nb_X (X = 0, 2, 4)$ metallic glasses in Hanks' solution were investigated by electrochemical polarization measurements. Polarization curves demonstrate that the addition of niobium into Zr–Co–Al amorphous alloys improves the corrosion resistance. Composition and chemical status of the elements in the passive film were characterized by XPS, and first-principles calculations based on density functional theory (DFT) were used to analyse the mechanism theoretically.

Keywords Metallic glasses · Corrosion · DOS · First-principles calculation

Introduction

Zr-based metallic glasses are expected to have medical applications as biomaterials, due to their high glass-forming ability (GFA), high strength and elastic strain limit, relatively low Young's modulus and excellent corrosion resistance [1–4]. Since the Inoue group has developed a nickel- and copper-free glassy Zr–Co–Al ternary alloy with a large supercooled liquid region and good mechanical properties [5], more and more attention has been paid to these metallic glasses. For medical and other applications, the corrosion resistance of the glassy Zr–Co–Al alloy needs to be evaluated and further improved.

✉ W. K. Le
lwk_lut@126.com

[1] State Key Laboratory of Advanced Processing and Recycling of Non-ferrous Metals, Lanzhou University of Technology, Lanzhou 730050, Gansu, China

It has been reported that addition of alloying element can remarkably enhance the corrosion resistance of some Zr-based metallic glasses, and to analyse how alloying affects the corrosion resistance of metallic glasses, X-ray photoelectron spectroscopy (XPS) was used to judge the composition of the passive film [6–8]. Unfortunately, these complex amorphous structures pose so big challenge to researcher that almost no report about theoretical analysis of how alloying affects the corrosion resistance of master alloy can be seen.

This work addresses two questions. First, which structural model was used to describe the amorphous structure? cluster packing that characterized by the icosahedral order proposed previously for some simpler metallic glasses? Second, how to conduct a theoretical analysis of alloying have an effect on the corrosion resistance of master alloy.

In this paper, Niobium was chosen as the doped element in Zr–Co–Al system. The corrosion resistance of the Nb-modified metallic glasses was tested in artificial body fluid by electrochemical polarization measurement. First-principles calculations based on density functional theory (DFT) were first used to analyse the result [9]. The new metallic glasses are promising for biomedical use; the present results provide a reference for investigating the corrosion resistance based on electron theory.

Experiment

Experiment procedure

The alloy ingots with the nominal compositions of $(Zr_{56}Al_{16}Co_{28})_{100-X}Nb_X (X = 0, 2, 4)$ were prepared by arc melting mixtures of the pure metals (the purity is above 99.9%) in an argon atmosphere. Each ingot was then

reversed and remelted four times to ensure chemical homogeneity. From the alloy ingots, ribbon samples with a cross-section of 0.05×3 mm^2 were fabricated by melt spinning. The structure of the specimens was examined by X-ray diffraction (XRD, Rigaku D/max-2400) using Cu Kα radiation at tube voltage of 40 kV and tube current of 150 mA. The thermal stability associated with glass transition, supercooled liquid, and crystallization for the glassy alloys was investigated by differential scanning calorimetry(DSC, NETZSCH STA 449F3) at a heating rate of 20 K/min in an argon atmosphere.

For electrochemical corrosion tests, electrochemical polarization was conducted in a three-electrode cell composed of a working electrode, a saturated calomel reference electrode (SCE), and a platinum counter electrode. The electrolyte used was Hanks' solution (a simulated body fluid) with pH 7.4 open to air, which was prepared from reagent-grade chemicals and deionized water. The potentiodynamic polarization curves of the specimens were recorded at a potential sweep rate of 1 mV/s when the open-circuit potential became almost steady after immersion in Hanks' solution for at least 20 min, which is 8.0 g/L·NaCl, 0.1 g/L $MgSO_4{\cdot}7H_2O$, 0.4 g/L KCl, 0.1 g/L $MgCl_2{\cdot}6H_2O$, 0.14 g/L·$CaCl_2$, 0.152 g/L $Na_2HPO_4{\cdot}12H_2O$, 0.06 g/L·KH_2PO_4, 1 g/L·$C_6H_{12}O_6$. The fracture surface was examined by scanning electron microscopy (SEM, JEOL JSM-6700F).

Experimental results and discussion

Figure 1 shows DSC curves of the melt-spun $(Zr_{56}Al_{16}Co_{28})_{100-X}Nb_X(X = 0, 2, 4)$ glassy alloy ribbons. All the alloys exhibit the sequent transition of glass transition, followed by supercooled liquid region and then crystallization, accompanying the distinctly separated two exothermic peaks. No appreciable difference in crystallization process is recognized between the melt-spun ribbon alloys, indicating the formation of a similar glassy phase.

The outer surfaces were smooth, and no trace of precipitation of crystalline phase was seen. The absence of a crystalline phase in the ribbon alloys was confirmed by X-ray diffraction [10]. X-ray diffraction patterns of the ribbon alloys exhibit no diffraction peak corresponding to a crystalline state, as shown in Fig. 2.

Figure 3 shows the potentiodynamic polarization curves of $(Zr_{56}Al_{16}Co_{28})_{100-X}Nb_X(X = 0, 2, 4)$ amorphous alloys in Hanks' solution; there is no obvious passivation region but pitting directly. The Nb-free sample shows lowest corrosion potential (E_{corr}) and highest corrosion current density (I_{corr}), but with minor addition of niobium E_{corr} increases and I_{corr} decreases. As we know, the value of E_{corr} indicates the corrosion tendency, while the value of I_{corr} indicates the corrosion rate. Higher E_{corr} indicates a small tendency to corrosion, while a low I_{corr} indicates a slow corrosion rate when a corrosion occurs. The corrosion data including the corrosion potential (E_{corr}) and the corrosion current density (I_{corr}) are summarized in Table 1. It can be concluded that the addition of niobium to Zr–Co–Al amorphous alloys can improve the corrosion resistance [11].

To better understand the corrosion mechanism of the Zr–Co–Al–Nb amorphous alloy, the samples were immersed in 3.5% solutions for 186 days; then, the composition and chemical status of the elements in the passive film were characterized by XPS, as shown in Fig. 4.

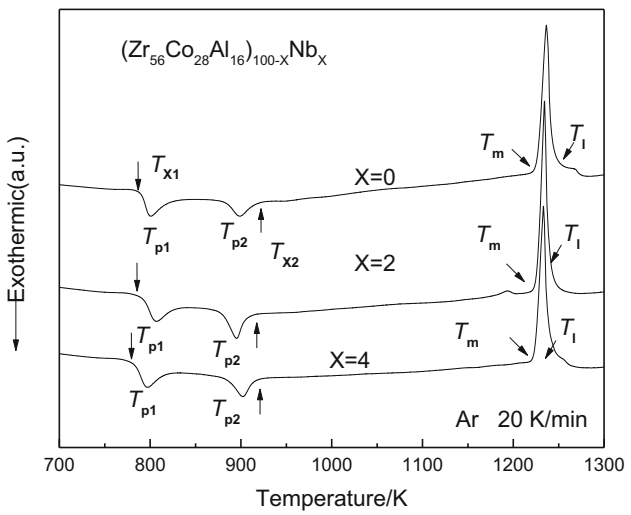

Fig. 1 DSC curves of $(Zr_{56}Al_{16}Co_{28})_{100-X}Nb_X(X = 0, 2, 4)$ alloy ribbons at heating rate of 20 K/min

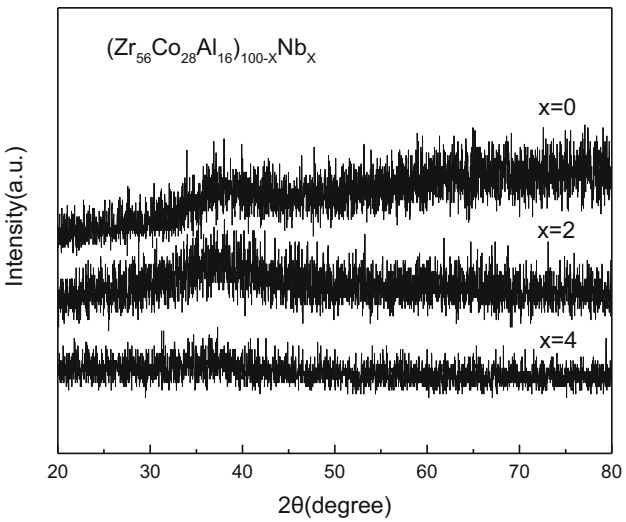

Fig. 2 XRD patterns of $(Zr_{56}Al_{16}Co_{28})_{100-X}Nb_X(X = 0, 2, 4)$ alloy ribbons

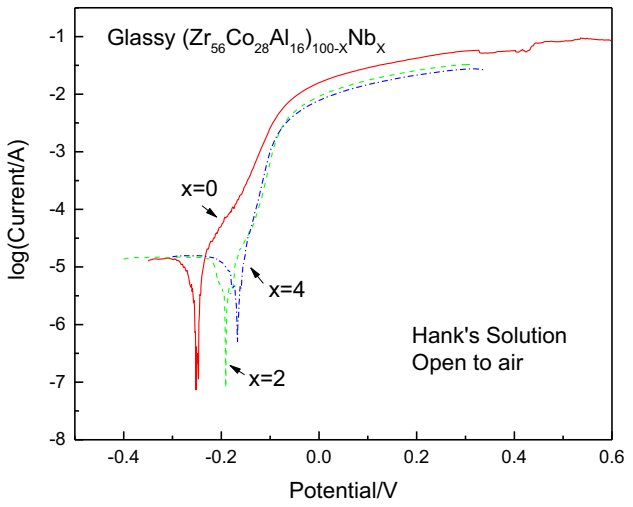

Fig. 3 Polarization curves for $(Zr_{56}Al_{16}Co_{28})_{100-X}Nb_X(X = 0, 2, 4)$ amorphous alloy in Hank's solution

Table 1 Values of E_{corr} and I_{corr} for $(Zr_{56}Al_{16}Co_{28})_{100-X}Nb_X(X = 0, 2, 4)$ amorphous alloy in Hank's solution

Samples	E_{corr}/V	$I_{corr}/\times 10^{-6}$A cm^{-2}
Nb0	−0.248	11.780
Nb2	−0.189	5.418
Nb4	−0.167	3.113

The Zr 3d spectrum consists of two peaks by multiplet splitting approximately at 182.21 and 184.82 eV, which can be assigned to Zr $3d_{5/2}$ and Zr $3d_{3/2}$ electrons originating from Zr^{4+} oxide state (ox). The Al 2p spectrum was decomposed into three spectra peaked at 71.42 eV corresponding to Al $2p_{3/2}$ electrons from metallic state, while, at 73.62 and 74.40 eV, Al $2p_{3/2}$ electrons from Al^{3+} oxide state. The O 1 s spectrum is fitted by two peaks, at 530.53 and at 532.31 eV assigned to metal oxide and Al_2O_3, respectively. Also, very little Co (about 0.3%) was detected in XPS, which is believed not to play a critical role in the outer passive film [7].

It has been reported previously that the high corrosion resistance of the Nb-doped Zr–Co–Al glass alloys is attributed to their single glass phase nature and formation of Zr^{4+}-and Al^{3+}-enriched oxide surface film in the corrosive solutions. XPS analysis revealed that the oxides formed on the sample surface consist mainly of Zr-oxide and Al-oxide for both Nb-free and Nb-bearing metallic glasses. As compared with the Nb-free metallic glasses, the addition of Nb increases significantly the amount of Zr-oxide, but slightly decreases the amount of Al-oxide. The two kinds of oxides are of a dense, compact and stable structure, and have a highly protective ability against corrosion; however, in the chloride ion contained solution,

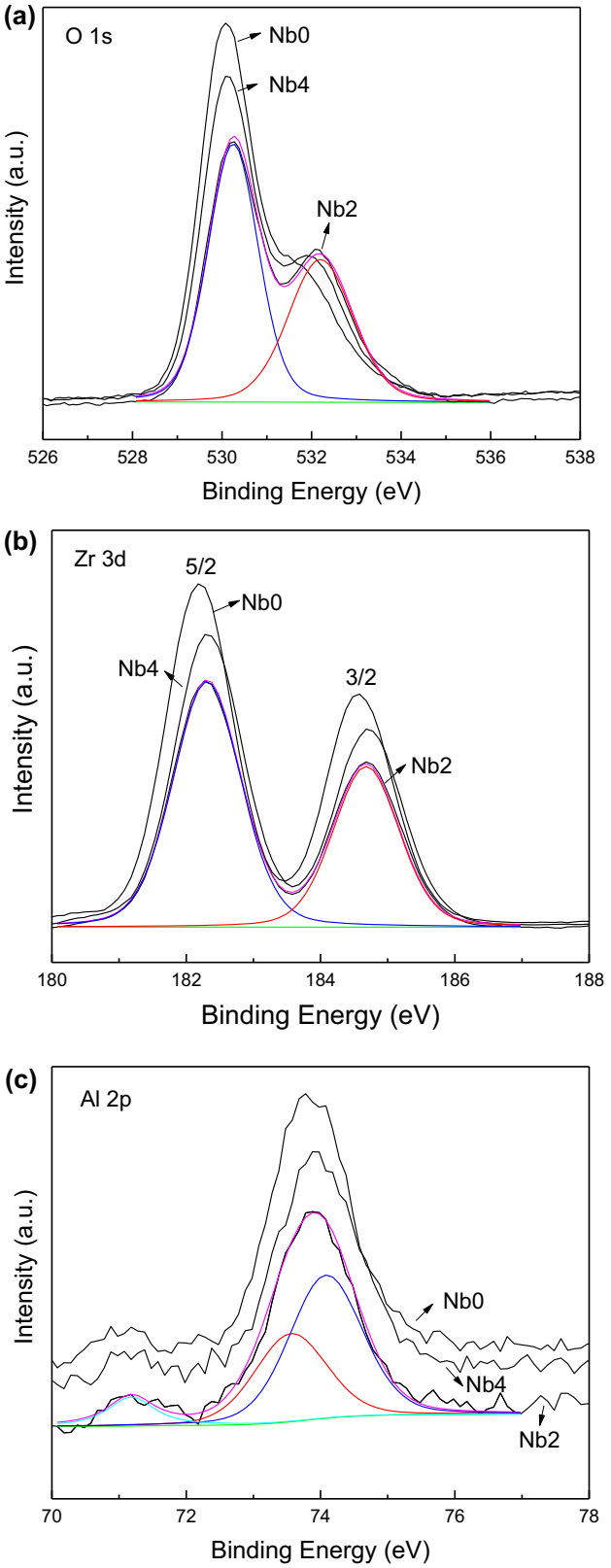

Fig. 4 XPS spectra of Zr 3d, Al 2p, Co 2p, O 1 s electrons of $(Zr_{56}Al_{16}Co_{28})_{100-X}Nb_X(X = 0, 2, 4)$ amorphous alloy: **a** O 1 s, **b** Zr 3d, **c** Al 2p. The *black curves* represent raw XPS spectra, and the *colored one fitted curves*

Zr-oxide is more protectable than Al-oxide; a direct comparison on the corrosion resistance between pure Zr and pure Al in chloride medium revealed higher pitting resistance of Zr than that of Al, suggesting that Zr-oxide was more stable than Al-oxide. Increasing Zr content and decreasing Al content in the surface films could enhance the corrosion resistance of those Zr-based amorphous alloy in chloride medium [12]. Thus, the addition of Nb is favorable for the amorphous alloy to form a protective surface film with higher chemical stability resulting in higher corrosion resistance in chloride medium.

However, the reason why Nb addition suppressed the formation of Al oxides, but promoted the formation of Zr-oxide is still unknown, which needs more comprehensive investigations.

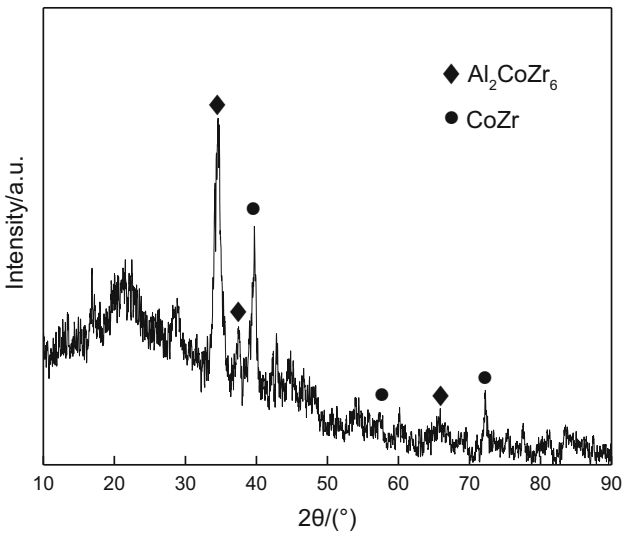

Fig. 5 XRD patterns of $Zr_{56}Al_{16}Co_{28}$ amorphous alloy after heating to 900 K

Calculation

Calculation model

For metallic glasses, to explain their macroscopic properties, it is important to understand their internal structure. Even though scholars proposed that some simpler amorphous structures can be described in terms of cluster packing characterized by the icosahedral order, it is not applicable to the structure of multicomponent metallic glasses. What is more, supposing metallic glasses can be seen as consisting of single cluster packing, when the single cluster packing was considered as a whole, its spatial arrangement must comply with laws, which is not consistent with the fact that amorphous alloy has long-range disorder. Thus, any single structure or cluster is not appropriate to describe amorphous structures, and the description of the atomic structure in an amorphous alloy cannot be exact.

The Inoue group in Sendai has developed the Zr–Al–Co alloy system. Wada et al. [13] found that the differential thermal analysis (DTA) curves of $Zr_{56}Al_{16}Co_{28}$, $Zr_{57}Al_{15}Co_{28}$ and $Zr_{58}Al_{14}Co_{28}$ amorphous alloy approximately the same, indicating the formation of a similar glassy phase. The microstructure of $Zr_{57}Al_{15}Co_{28}$ alloy may consist of ZrCo and Zr_6Al_2Co and small-volume fraction of ZrAlCo phases. With deviating alloy compositions from $Zr_{57}Al_{15}Co_{28}$, the alloys that melted and solidified with the similar phases were confirmed by crystallization process, which is consistent with the reported ternary equilibrium phase diagram [14]. Figure 5 shows the XRD patterns of $Zr_{56}Al_{16}Co_{28}$ amorphous alloy after heating to 900 K with a heating rate of 20 K/min; no Zr–Al–Co phase was found, which was probably because the amount was so small.

The amorphous alloy has long-range disorder, special structure of the short-range order. When amorphous alloys are crystallized, corresponding crystalline phase was produced. The atomic arrangement in short-range of an amorphous alloy tends to be the same as the atomic arrangement of the corresponding crystalline phase; otherwise, atomic arrangement cannot change from disorder to order immediately when crystallized. The amorphous alloy is constituted of quasi-equivalent cluster.

To investigate the structure of amorphous alloy, a simple and accurate method based on quasi-equivalent cluster was proposed. The $Zr_{56}Al_{16}Co_{28}$ amorphous alloy is constituted of α quasi-equivalent cluster, β quasi-equivalent cluster and γ quasi-equivalent cluster, and the atomic arrangement of α quasi-equivalent cluster, β quasi-equivalent cluster, and γ quasi-equivalent cluster is similar to ZrCo phase, Zr_6Al_2Co phase, and ZrAlCo phase, respectively, but these clusters in amorphous alloy are disorganized. Why this method can work well with the challenge we face? This method can well explain at least the following three basic questions. First, when the alloy melted and solidified, the microstructure of $Zr_{57}Al_{15}Co_{28}$ alloy consists of ZrCo and Zr_6Al_2Co and small-volume fraction of Zr–Al–Co phases. Second, amorphous alloy has long-range disorder, special structure of the short-range order; so, amorphous structures described in terms of cluster packing characterized by the icosahedral order is meaningful only in the statistical sense. Third, the description of the atomic structure in amorphous alloy cannot be exact; the atomic-level structure of amorphous alloy remains elusive and intriguing.

Doping position

When alloying element Niobium was added to $Zr_{56}Al_{16}Co_{28}$ amorphous alloy, it is easier to substituted atomic,

since $r_{Zr} = 0.160$ nm, $r_{Co} = 0.126$ nm, $r_{Al} = 0.143$ nm, $r_{Nb} = 0.148$ nm, the gap of atomic radius of Nb and Zr, Nb and Al is small, and Nb is next to Zr in the periodic table of chemical elements. If the element Nb is interstitial atom, the lattice distortion can be high; so, cluster becomes unstable.

Table 2 shows the calculation results of Nb-doped α quasi-equivalent cluster supercell systems. From these figures, we may see that binding energy of Nb atom substitutes for the position of Zr atom is lower than Co atom. Table 3 shows the calculation results of Nb-doped β quasi-equivalent cluster supercell systems; from the table, we know that binding energy of Nb atom substitutes for the position of Zr atom is the lowest; therefore, it is easier for Nb atom substitutes for the position of Zr atom.

Calculation results and discussion

Figure 6a is the spatial structure of α quasi-equivalent cluster; Fig. 6b is the spatial structure of β quasi-equivalent cluster, and γ quasi-equivalent cluster was not considered in this study, since it is far few in amorphous alloy. The density of states (DOS) calculations were performed within the framework of the generalized gradient approximation (GGA), as implemented within the CASTEP, a density functional plane-wave pseudopotential program in Materials Studio. PW91 was employed for the exchange correlation functional. An energy cut-off of 300 eV was used for the plane-wave expansion. For geometric optimization, the Brillion zone integration was sampled using a 4 × 4 × 8 Γ-centered k-point grid.

Figure 7 shows the partial density of states (PDOS) of β quasi-equivalent cluster with different doping ratios of niobium which were calculated using LDA. It is shown in Fig. 6a that the majority contribution of PDOS is from the d states of Zr. When niobium doped β quasi-equivalent cluster with 2%, the sharp peak appears at the Fermi level in the spin-up region for Zr-d atoms. When it comes to 4%, the sharp peak appears at low-energy states for Zr-d atoms. The Al-s and Al-p atoms make a small contribution as shown in Fig. 7c. The contribution of Co atoms is very small at the conduction region (Fig. 7b). Figure 8 summarizes the results of the PDOS of α quasi-equivalent cluster with different doping ratios of niobium. Similar to Fig. 7, the majority contribution of PDOS is from the d states of Zr.

When niobium was added to Zr–Co–Al metallic glass, its was improved. Since the amount of niobium is very small, it is impossible to change the crystal structure in the long-range. When niobium was added to Zr–Co–Al metallic glasses, spatial structure of the atoms within short-range was changed, Fermi level is higher, atoms especially Zr–d are more active, which makes it easier for the passivation film to produce and changes the structure of protective surface layers; thus, the corrosion resistance

Table 2 Total energy and difference between binding energy of Nb-doped α quasi-equivalent cluster supercell systems (eV)

Supercell	$E_{tot}(Zr_{n-1}Co_nNb)$	$E_{tot}(Zr)$	E_{tot}
2 × 2 × 2	−18868.71	−2548.18	−21416.89
2 × 2 × 1	−9568.84	−2548.18	−12117.02
1 × 2 × 1	−4919.10	−2548.18	−7467.28
Supercell	$E_{tot}(Zr_nCo_{n-1}Nb)$	$E_{tot}(Co)$	E_{tot}
2 × 2 × 2	−19106.40	−2072.15	−21178.55
2 × 2 × 1	−9806.42	−2072.15	−11878.57
1 × 2 × 1	−5156.50	−2072.15	−7228.65

Table 3 Total energy and difference between binding energy of Nb-doped β quasi-equivalent cluster supercell systems (eV)

Supercell	$E_{tot}(Zr_{6n-1}Co_nAl_{2n}Nb)$	$E_{tot}(Zr)$	E_{tot}
2 × 2 × 2	−71037.02	−2548.18	−73585.20
2 × 2 × 1	−35654.22	−2548.18	−38202.40
1 × 2 × 1	−17962.14	−2548.18	−20510.32
Supercell	$E_{tot}(Zr_{6n}Co_{n-1}Al_{2n}Nb)$	$E_{tot}(Co)$	E_{tot}
2 × 2 × 2	−71273.25	−2072.15	−73345.40
2 × 2 × 1	−35890.03	−2072.15	−37962.18
1 × 2 × 1	−18198.02	−2072.15	−20270.17
Supercell	$E_{tot}(Zr_{6n}Co_nAl_{2n-1}Nb)$	$E_{tot}(Al)$	E_{tot}
2 × 2 × 2	−72260.95	−105.18	−72366.13
2 × 2 × 1	−36877.56	−105.18	−36982.74
1 × 2 × 1	−19185.49	−105.18	−19290.67

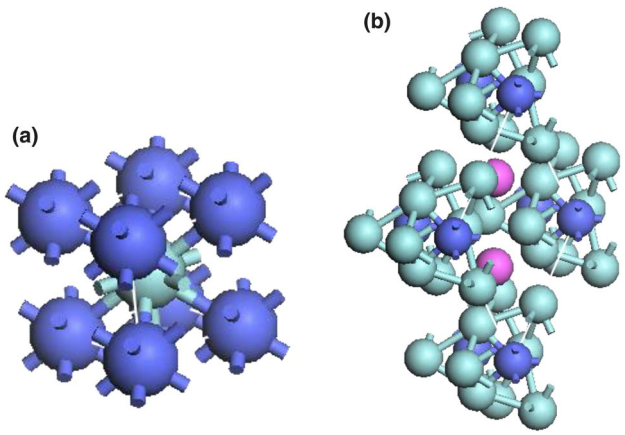

Fig. 6 Spatial structure of quasi-equivalent cluster: **a** α, **b** β

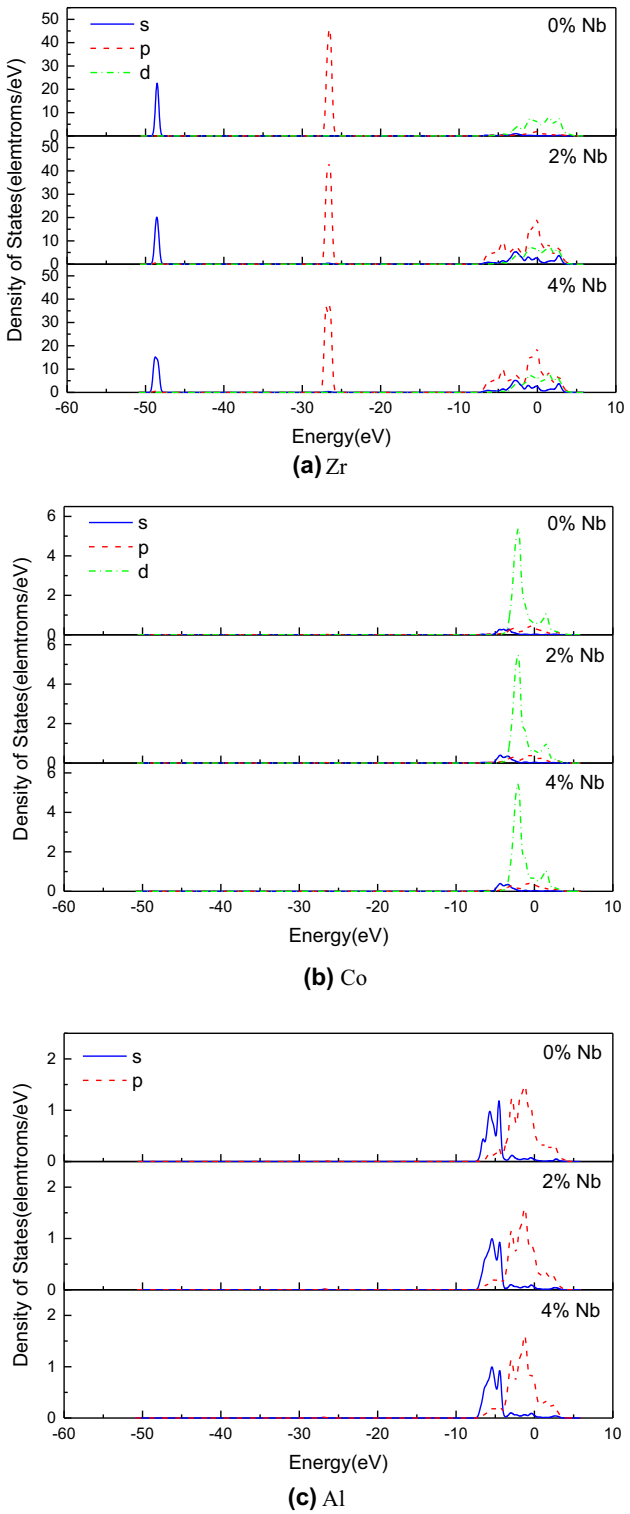

Fig. 7 Partial density of states(PDOS) of β quasi-equivalent cluster with doping ratio of niobium **a** Zr, **b** Co, **c** Al

ability was better. The calculation results are consistent with the experimental results, but how the niobium changes the arrangement of extranuclear electrons of

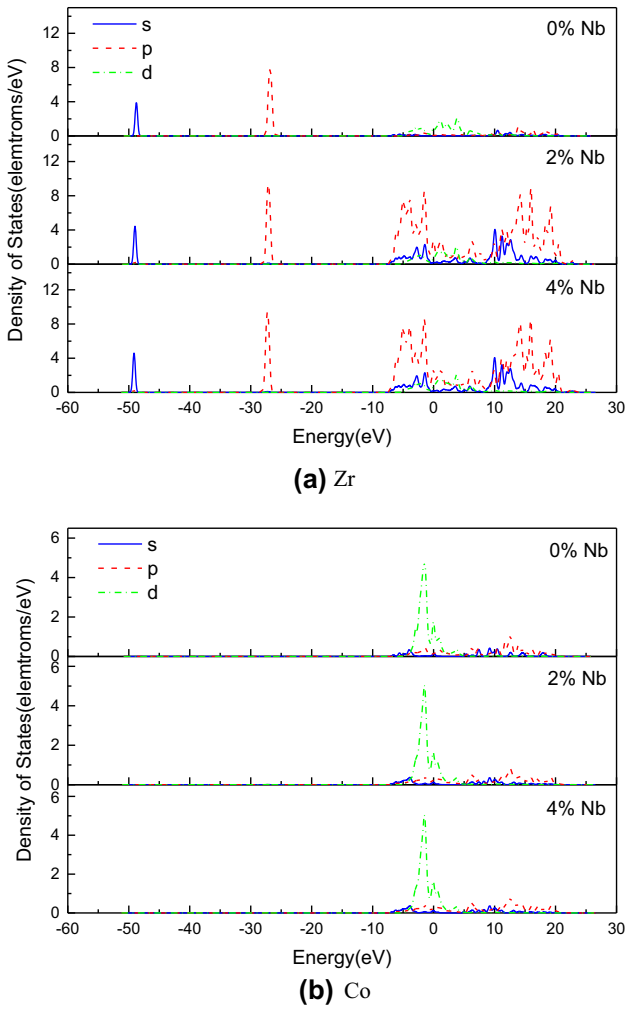

Fig. 8 Partial density of states (PDOS) of α quasi-equivalent cluster with different doping ratios of niobium, **a** Zr, **b** Co

atoms is still unknown, which needs more comprehensive investigations.

Conclusions

The effects of niobium addition on corrosion resistance of Zr–Co–Al ternary metallic glasses were investigated; results show that the addition of niobium into Zr–Co–Al amorphous alloys makes the value of I_{corr} lower, decreases the corrosion rate, and improves the corrosion resistance. XPS analysis revealed that the addition of Nb increases significantly the amount of Zr-oxide, but slightly decreases the amount of Al-oxide in the surface films. First-principles calculations based on density functional theory (DFT) were used to analyse the result. Niobium-doped amorphous alloy makes Zr–d more active, which may change the structure of passive film; thus, corrosion resistance was improved.

References

1. Inoue, A.: Acta Mater. **48**, 279–306 (2000)
2. Li, Y.H., Zhang, W., Dong, C., Qiang, J.B., Xie, G.Q., Fujita, K., Inoue, A.: J. Alloys Compd. **536S**, S117–S121 (2012)
3. Zhang, B., Liao, S., Shu, X., Xie, H.: J. Theor. Appl. Phys. **10**, 129–137 (2016)
4. Li, Y.H., Zhang, W., Dong, C., Qiang, J.B., Fukuhara, M., Makino, A., Inoue, A.: Mater. Sci. Eng. A **528**, 8551–8556 (2011)
5. Zhang, T., Inoue, A.: Mater. Trans. **43**, 267–270 (2002)
6. Kawashima, A., Wada, T.K.: Ohmura, Xie, G.Q., Inoue, A. Mater. Sci. Eng. A **5422**, 140–146 (2012)
7. Zhang, C., Li, N., Pan, J., Guo, S.F., Zhang, M., Liu, L.: J. Alloys Compd. **504S**, S163–S167 (2010)
8. Qin, C.L., Zeng, Y.Q., Louzguine, D.V., Nishiyama, N., Inoue, A.: J. Alloys Compd. **504S**, S172–S175 (2010)
9. Afshar, M., Babaei, M., Kordbacheh, A.H.: J. Theor. Appl. Phys. **8**, 59 (2014)
10. Pang, S.J., Zhang, T., Asami, K., Inoue, A.: J. Mater. Res. **18**, 1652–1658 (2003)
11. Pi, J.H., Pan, Y., Wu, J.L., He, X.C.: Rare Met. Mater. Eng. **43**, 0032–0035 (2014)
12. Hua, N., Huang, L., Chena, W.Z., He, W., Zhang, T.: Mater. Sci. Eng. C **44**, 400–410 (2014)
13. Wada, T., Qin, F.X., Wang, X.M., Yoshimura, M., Inoue, A.: Mater. Res. Soc. **24**, 2941–2948 (2009)
14. ASM Alloy Phase Diagrams Center: http://www.asminternational.org/asmenterprise/apd/. Accessed 16 June 2015